# REPORT DOCUMENTATION PAGE

*Form Approved*
*OMB No. 0704-0188*

The public reporting burden for this collection of information is estimated to average 1 hour per response, including the time for reviewing instructions, searching existing data sources, gathering and maintaining the data needed, and completing and reviewing the collection of information. Send comments regarding this burden estimate or any other aspect of this collection of information, including suggestions for reducing the burden, to Department of Defense, Washington Headquarters Services, Directorate for Information Operations and Reports (0704-0188), 1215 Jefferson Davis Highway, Suite 1204, Arlington, VA 22202-4302. Respondents should be aware that notwithstanding any other provision of law, no person shall be subject to any penalty for failing to comply with a collection of information if it does not display a currently valid OMB control number.
**PLEASE DO NOT RETURN YOUR FORM TO THE ABOVE ADDRESS.**

| 1. REPORT DATE *(DD-MM-YYYY)* | 2. REPORT TYPE | 3. DATES COVERED *(From - To)* |
|---|---|---|
| 9/30/07 | Final Technical Report | 2/1/04-6/30/07 |

**4. TITLE AND SUBTITLE**
High-Order Accurate Time-Domain Electromagnetics and PCS Prediction for Dynamic and Uncertain Scatters

**5a. CONTRACT NUMBER**

**5b. GRANT NUMBER**
FA9550-04-1-0072

**5c. PROGRAM ELEMENT NUMBER**

**6. AUTHOR(S)**
Jan S. Hesthaven

**5d. PROJECT NUMBER**

**5e. TASK NUMBER**

**5f. WORK UNIT NUMBER**

**7. PERFORMING ORGANIZATION NAME(S) AND ADDRESS(ES)**
Applied Math/Brown University
182 George St.
Providence, RI 02912

**8. PERFORMING ORGANIZATION REPORT NUMBER**

**9. SPONSORING/MONITORING AGENCY NAME(S) AND ADDRESS(ES)**
Air Force Office of Scientific Research
875 North Randolph St., Suite 325
Arlington, VA 22203
Dr John Schmisseur/NA

**10. SPONSOR/MONITOR'S ACRONYM(S)**

**11. SPONSOR/MONITOR'S REPORT NUMBER(S)**
AFRL-SR-AR-TR-08-0041

**12. DISTRIBUTION/AVAILABILITY STATEMENT**
Approved for public release,
distribution unlimited

**13. SUPPLEMENTARY NOTES**

**14. ABSTRACT**
In this project we have pursued the development of computational ways of quantifying the impact of uncertainties on RCS computation. We present a systematic, accurate, and efficient way of addressing such problem, essentially enabling one to compute with an ensample of data and, subsequently, obtain a full space-time ensample of solutions with an associated probability density.

The uncertainties can be present in the sources, the materials, or the geometries.

**15. SUBJECT TERMS**

| 16. SECURITY CLASSIFICATION OF: | | | 17. LIMITATION OF ABSTRACT | 18. NUMBER OF PAGES | 19a. NAME OF RESPONSIBLE PERSON |
|---|---|---|---|---|---|
| a. REPORT | b. ABSTRACT | c. THIS PAGE | | 23 | 19b. TELEPHONE NUMBER *(Include area code)* |

Final report on AFOSR T&E effort FA9550-04-1-0072

# High-Order Accurate Time-Domain Electromagnetics and RCS Prediction for Dynamic and Uncertain Scatterers

Jan S Hesthaven
Division of Applied Mathematics
Brown University, Box F
Providence, RI 02912

Phone : (401) 863 2671,
Fax : (401) 863 1355
Email : Jan.Hesthaven@Brown.edu

September 30, 2007

20080131283

# 1 Introduction and Overview

While computational methods have become increasingly refined and accurate, their reliance on exact data, e.g., complete descriptions of geometries, materials, sources, etc., is emerging as a bottleneck in the modeling of problems of realistic complexity. For instance, if one attempts to model an experiment, a classic computational approach would require knowledge of a degree of detail which is unrealistic and often impossible to obtain, e.g., one cannot hope to control all elements of an experiment, measure all details of an initial condition or geometry, know the microstructure of all materials, etc.

The usual approach to dealing with this lack of knowledge or uncertainty is to simply assume some mean parameters and compute the corresponding solution. If the solution is robust to parameter variation, this is indeed a reasonable approach. However, for general problems, where the sensitivity of parts of the solution can be significant, a solution based on mean parameters is not likely to match very well with experiments and, thus, is not a good predictive tool. An experimentalist would naturally deal with this exact problem by repeating the experiments and, subsequently, compute not only mean results but also error bars—reflecting, at least partly, the sensitivity of the solution.

It is natural to strive to achieve similar abilities in computational modeling effort, e.g., compute solutions or measures of interest and their associated sensitivities. Clearly, if a particular measured entity is highly sensitive there is no reason to expect that this matches experiments exactly. Thus, we would like to be able to model the impact of the uncertainty, assumed to have certain properties derived from experiments or otherwise, on the computed results, essentially resulting in an ensample of possible solution values with an associated probability. This would immediately enable the computation of statistical moments, e.g., means and variances, and of other valuable information about the sensitivity of solutions and derived quantities.

In this project we have pursued this goal and we present here a systematic, accurate, and efficient way of addressing this type of problem, essentially enabling one to compute with an ensample of data and, subsequently, obtain a full space-time ensample of solutions with an associated probability density. It is important to realize that is this not a simple situation, since solutions may vary nonlinearly in the uncertainty due to stochastic correlations even if the deterministic problem is linear, e.g., Maxwell's equations.

A standard way of addressing problems of the type mentioned in the above is through Monte Carlo sampling, e.g., run a deterministic code a large number of times and, subsequently, extract the statistics of interest. The main problem with this approach is the very slow convergence rate, $\mathcal{O}(N^{-1/2})$, with $N$ being the number of samples, which makes even the computation of mean solutions expensive and accurate recovery of higher moments, e.g., variances, prohibitive.

Our platform on which to demonstrate this approach is the time-domain Maxwell's equations, solved using a high-order accurate discontinuous Galerkin method. However, the basic elements of the formulation are general and can be used with any computational kernel.

We have focused on the development of efficient and accurate means by which to provide quantitative measures on the impact on the radar cross section by uncertainties in general scattering problems. The uncertainties can be present in the sources, the materials, or the geometries.

A summary of the main accomplishments are

- Validated the use of Wiener chaos expansion methods for a variety of Maxwell benchmark problems, including internal, external, time-domain, and harmonic problems.

- Developed a collocation form of the chaos expansion method to dramatically decrease the computational cost of using such methods.
- Developed the chaos techniques to enable the modeling to uncertain sources, materials, and geometries. The latter has resulted in the introduction of a new stochastic mapping technique to enable the modeling of general scatterers.
- Developed techniques to model spatially correlated uncertainty based on statistical knowledge of the uncertainty.
- Developed a theoretical understanding of the convergence rate and long time behavior of the chaos expansion methods.
- Demonstrated the ability to apply such techniques to quantify the impact of uncertainty on scattering problems and the resulting sensitivity of the RCS.

In the following we shall elaborate a little more on some of these many aspects.

## 2 Maxwell's equations

Let us consider a general domain $\Omega$ and let $\mathbf{E}^s$ and $\mathbf{H}^s$ denote the scattered electric and magnetic fields, respectively. With $\varepsilon(\mathbf{x})$ and $\mu(\mathbf{x})$ being the local permittivity and permeability, and $\sigma(\mathbf{x})$ the conductivity of the media, the time-dependent Maxwell's equations in the scattered field formulation are given as

$$\epsilon \frac{\partial \mathbf{E}^s}{\partial t} = \nabla \times \mathbf{H}^s + \sigma \mathbf{E}^s + \mathbf{S}^E, \tag{1}$$

$$\mu \frac{\partial \mathbf{H}^s}{\partial t} = -\nabla \times \mathbf{E}^s + \mathbf{S}^H, \tag{2}$$

where, as is common in time-domain schemes, we have neglected divergence constraints, assuming that these amount to constraints on the initial conditions.

The source terms, $\mathbf{S}^E$ and $\mathbf{S}^H$, appearing on the right-hand side of (1)–(2), take the form

$$\mathbf{S}^E = -(\epsilon - \epsilon^i)\frac{\partial \mathbf{E}^i}{\partial t} + (\sigma - \sigma^i)\mathbf{E}^i, \tag{3}$$

$$\mathbf{S}^H = -(\mu - \mu^i)\frac{\partial \mathbf{H}^i}{\partial t}, \tag{4}$$

where the incident field $(\mathbf{E}^i, \mathbf{H}^i)$ is a solution to Maxwell's equations in a media of permittivity, permeability, and conductivity—$\varepsilon^i(\mathbf{x})$, $\mu^i(\mathbf{x})$, $\sigma^i(\mathbf{x})$, respectively.

We now turn our attention to boundary conditions. Along a perfect electric conductor (PEC), the boundary conditions on the electric field are

$$\hat{\mathbf{n}} \times \mathbf{E}^t = \mathbf{0}, \tag{5}$$

where $\hat{\mathbf{n}}$ is the outward pointing normal vector at the surface and $\mathbf{E}^t = \mathbf{E}^i + \mathbf{E}^s$ is the total field. For the total magnetic field $\mathbf{H}^t$, the condition is

$$\mathbf{H}^t \cdot \hat{\mathbf{n}} = 0. \tag{6}$$

Along the interface of two dielectric bodies, denoted by the subscripts 1 and 2, we have

$$\hat{\mathbf{n}} \times (\mathbf{E}_1^s - \mathbf{E}_2^s) = \mathbf{0} \text{ and } \hat{\mathbf{n}} \times (\mathbf{H}_1^s - \mathbf{H}_2^s) = \mathbf{0}; \tag{7}$$

i.e., all tangential components are continuous.

## 3 Numerical scheme for the deterministic case

Before turning our attention to the case including uncertainties, let us briefly describe the computational methods used for solving Maxwell's equations in the physical space. We use a discontinuous Galerkin formulation; the solution will be discontinuous between elements. This offers a number of advantages over widely used alternative techniques, e.g., geometric flexibility through fully unstructured grids, high-order accuracy to enable accurate wave propagation over long distance with a coarse resolution, and very high computational efficiency through explicit time stepping and high parallel performance. The method has been discussed, analyzed, and validated extensively for Maxwell's equations and we shall simply sketch its main components.

We rewrite Maxwell's equations (1)–(2) in conservation form

$$Q\frac{\partial \mathbf{q}}{\partial t} + \nabla \cdot \mathbf{F}(\mathbf{q}) = \mathbf{S}, \tag{8}$$

where $\mathbf{q}$ is the state vector formed by the scattered electric field and the magnetic field

$$\mathbf{q} = \begin{pmatrix} \mathbf{E} \\ \mathbf{H} \end{pmatrix}, \tag{9}$$

and the components of the tensor $\mathbf{F}$ are defined by

$$\mathbf{F}_i(\mathbf{q}) = \begin{pmatrix} -\mathbf{e}_i \times \mathbf{H} \\ \mathbf{e}_i \times \mathbf{E} \end{pmatrix}, \tag{10}$$

where $\mathbf{e}_i$ denotes the Cartesian unit vectors. On the right-hand side of (8), $\mathbf{S} = [\mathbf{S}^E, \mathbf{S}^H]$ is the source term, which depends on the incident field, and the material matrix $Q$ is a diagonal matrix with values $(\epsilon, \epsilon, \epsilon, \mu, \mu, \mu)$ on its diagonal.

We assume that the computational domain, $\Omega$, is tessellated by triangles or tetrahedrons, $D$, and we represent the local solution $\mathbf{q}_N$ as

$$\mathbf{q}_N(\mathbf{x}, t) = \sum_{i=1}^{N} \widetilde{\mathbf{q}}_i(t) L_i(\mathbf{x}), \tag{11}$$

where $\widetilde{\mathbf{q}}_i$ reflects nodal values, defined on the element, and $L_i(\mathbf{x})$ signifies an $n$th order Lagrange polynomial, associated with grid points.

The discrete solution, $\mathbf{q}_N$, of Maxwell's equations is required to satisfy

$$\int_D \left( Q\frac{\partial \mathbf{q}_N}{\partial t} + \nabla \cdot \mathbf{F}(\mathbf{q}_N) - \mathbf{S}_N \right) L_i(\mathbf{x}) d\mathbf{x} = \oint_{\partial D} \hat{\mathbf{n}} \cdot [\mathbf{F}(\mathbf{q}_N) - \mathbf{F}^*] L_i(\mathbf{x}) d\mathbf{x}. \tag{12}$$

In (12), $\mathbf{F}^*$ denotes a numerical flux and $\hat{\mathbf{n}}$ is an outward pointing unit vector defined at the boundary $\partial D$ of the element $D$. Note that this is an entirely local formulation, and relaxing the continuity of the elements decouples the elements, resulting in a block-diagonal global mass matrix which can

be trivially inverted in preprocessing. The price to pay for this is the additional degrees of freedom needed to support the local basis functions. For high-order elements, this is, however, only a small fraction of the total number of degrees of freedom. Given the linearity of Maxwell's equations, and for stability reasons, it is natural to use an upwinding flux which takes the form

$$\hat{\mathbf{n}} \cdot [\mathbf{F}(\mathbf{q}_N) - \mathbf{F}^*] = \begin{pmatrix} \overline{Z}^{-1} \hat{\mathbf{n}} \times (\hat{\mathbf{n}} \times [\mathbf{E}_N] - Z^+ [\mathbf{H}_N]) \\ \overline{Y}^{-1} \hat{\mathbf{n}} \times (\hat{\mathbf{n}} \times [\mathbf{E}_N] - Z^+ [\mathbf{H}_N]) \end{pmatrix}, \tag{13}$$

where the bracket $[\mathbf{q}] = \mathbf{q}^- - \mathbf{q}^+$ denotes the jump in the field values ($\mathbf{q}^-$ is the local value and $\mathbf{q}^+$ is the neighboring value) across an interface, $Z^\pm$ is the local impedance, and $Y^\pm$ is the local conductance,

$$Z^\pm = \frac{1}{Y^\pm} = \sqrt{\frac{\mu^\pm}{\epsilon^\pm}}. \tag{14}$$

$\overline{Z}$ and $\overline{Y}$ in (13) are the sums

$$\overline{Z} = Z^+ + Z^-, \quad \overline{Y} = Y^+ + Y^-. \tag{15}$$

After discretization of the operators and evaluation of the integrals appearing in (12), the problem can be rewritten in matrix-vector form

$$QM \frac{d\mathbf{q}_N}{dt} + S \cdot \mathbf{F}_N - M\mathbf{S}_N = F\hat{\mathbf{n}} \cdot [\mathbf{F}_N - \mathbf{F}^*]. \tag{16}$$

The matrices $M$, $S$, and $F$ represent the local mass-, stiffness-, and face-integration matrices. Note that the local nature of the scheme allows for the use of an explicit solver for the time discretization of (16). This is traditionally done using an explicit Runge–Kutta method, although suitable alternatives are plentiful.

## 4 Accounting for the uncertainty

To deal with the actual lack of detailed knowledge leading to the uncertainty, we must make some educated guesses—a model—about the nature of the possible variations in the data. These models can be based on pure speculation, on measured data, or on other available information. Once this is done, however, we must introduce this into the computational approach in an efficient, accurate, and robust manner.

Consider, as a simple example, the wave equation

$$\frac{\partial u}{\partial t} + a(\theta) \frac{\partial u}{\partial x} = 0, \tag{17}$$

where $\theta$ is a random parameter with some associated probability density function (PDF). Thus, this represents an ensemble of wave problems, each with an individual phase speed occurring with a probability given by the PDF; i.e., the solution $u$ is not only a function of $(x, t)$ but also of $\theta$, and the equation is a stochastic wave equation.

The actual form of $a(\theta)$ may not be known, causing the introduction of the uncertainty. However, it seems quite reasonable that in many situations one can measure or conjecture the average of $a$ and perhaps its variation; i.e., one can reasonably assume that $a(\theta)$ varies in a certain way related to a normal distribution with a given mean and variance.

The question remains, however, how this uncertainty will affect the solution, $u(x,t,\theta)$, and, more often, its moments such as the mean and the variance. This is not a trivial question, as the uncertainty essentially renders the simple linear problem considerably more complex due to possible stochastic dependence between $a$ and $u$.

One could naturally solve the above problem for a large number of values of $\theta$, taken from a proper distribution, and, subsequently, compute the appropriate moments. This is the essence of a Monte Carlo method and suffers from a very slowly converging result as $1/\sqrt{N}$, with $N$ being the number of samples. If higher-order moments, e.g., the variance or sensitivity of the result, are required, this is often prohibitive.

In the above example, the uncertainty enters through the phase speed. However, as we shall see shortly, dealing with uncertainty in initial conditions, boundary conditions, sources, or computational domain/geometries can be done in an entirely similar fashion.

In this section, we shall discuss two variations, referred to as stochastic Galerkin and collocation, respectively, of the same underlying result. This enables one to discretize stochastic partial differential equations (SPDEs) to recover systems of deterministic problems which we can subsequently solve with the methods discussed later. As we shall experience through examples, both techniques offer excellent accuracy at a severely reduced computational cost as compared to straightforward Monte Carlo methods.

### 4.1 The homogeneous chaos expansion

The key result on which we shall rely is due to Wiener and shows that the chaos expansion can be used to approximate any functional in $L^2(\Omega,\mathcal{P})$, where $\mathcal{P}$ is a Gaussian measure on $\Omega$. For such a random variable $X(\theta)$, the chaos expansion is written as

$$\begin{aligned} X(\theta) &= a_0 H_0 \\ &\quad + \sum_{i_1=1}^{d} a_{i_1} H_1(\xi_{i_1}(\theta)) \\ &\quad + \sum_{i_1=1}^{d}\sum_{i_2=1}^{i_1} a_{i_1 i_2} H_2(\xi_{i_1}(\theta),\xi_{i_2}(\theta)) \\ &\quad + \sum_{i_1=1}^{d}\sum_{i_2=1}^{i_1}\sum_{i_3=1}^{i_2} a_{i_1 i_2 i_3} H_3(\xi_{i_1}(\theta),\xi_{i_2}(\theta),\xi_{i_3}(\theta)) \\ &\quad + \cdots, \end{aligned} \tag{18}$$

where $\xi = (\xi_1(\theta),\ldots,\xi_d(\theta))$ represents $d$ independent Gaussian variables with zero mean and unit variance, each depending on the random event $\theta$, and $H_n$ are the multivariate Hermite polynomials defined as

$$H_n(\xi_{i_1}(\theta),\ldots,\xi_{i_n}(\theta)) = e^{\frac{1}{2}\xi^T\xi}(-1)^n \frac{\partial^n}{\partial\xi_{i_1},\ldots,\partial\xi_{i_n}} e^{-\frac{1}{2}\xi^T\xi}. \tag{19}$$

The number of terms in the expansion (18) grows as

$$P = \frac{(n+d)!}{n!d!}, \tag{20}$$

where $n$ is the length of the Hermite expansion and $d$ is the dimension of the Gaussian random space. The polynomial homogeneous chaos expansion forms a complete orthogonal basis in the

space of Gaussian variables, i.e.,

$$\langle H_i(\xi_{i_1}(\theta),\ldots,\xi_{i_n}(\theta)), H_j(\xi_{j_1}(\theta),\ldots,\xi_{j_n}(\theta))\rangle \tag{21}$$

$$= \int_{R^d} \frac{H_i(\xi_{i_1}(\theta),\ldots,\xi_{i_n}(\theta))H_j(\xi_{j_1}(\theta),\ldots,\xi_{j_n}(\theta))}{\sqrt{(2\pi)^d}} e^{-\frac{1}{2}\xi^T\xi} d\xi = i!\delta_{ij},$$

where $i$ denotes the multi-index $(i_1,\ldots,i_n)$ and $i! = i_1!,\ldots,i_n!$. Thus there is an intimate relation between the Hermite polynomials, orthogonal under the Gaussian weight, and the representation of random variables taken from a Gaussian distribution. One way of interpreting the homogeneous chaos expansion is that a general random variable can be expressed in terms of simpler Gaussian variables for which we can construct an efficient computational approach. Clearly, if the random variable is far from Gaussian, many terms in the expansion will be needed; i.e., $n$ must be large. An alternative is to use an expansion in terms of other random variables with an associated distribution closer to what is expected at input or output. For notational convenience, we can rewrite (18) in the form

$$X(\theta) = \sum_{j=1}^{P} b_j \Psi_j(\xi), \tag{22}$$

where there is a one-to-one correspondence between the functions $H_i$ and $\Psi_j$ and also between the coefficients $a_{i_1,\ldots,i_p}$ and $b_j$. In the case of a general stochastic process, these coefficients will be time dependent.

To model the impact of uncertainty on the propagation of electromagnetic waves, we include the randomness in the usual spatial-temporal dimensions; i.e., the electric field and the magnetic field become $\mathbf{E}(\mathbf{x},t,\theta)$ and $\mathbf{H}(\mathbf{x},t,\theta)$, reflecting that the fields are functions of $d$ independent random variables, $(\xi_{i_1}(\theta),\ldots,\xi_{i_d}(\theta))$.

In the following we shall discuss in some detail how this can be utilized to construct an efficient computational method. For simplicity of the discussion, we assume in what follows that one Gaussian variable suffices to represent the process (i.e., $d = 1$). However, the formulation is general and applies to problems requiring many random variables to describe the stochastic processes.

### 4.2 Stochastic Galerkin formulation

Using the chaos expansion, we can express $\mathbf{q}(\mathbf{x},t,\theta) = (\mathbf{E}(\mathbf{x},t,\theta),\mathbf{H}(\mathbf{x},t,\theta))^T$ as

$$\mathbf{q}(\mathbf{x},t,\theta) = \sum_{i=1}^{P} \mathbf{q}^i(\mathbf{x},t)\Psi_i(\theta). \tag{23}$$

We can write the computational scheme, which takes into account randomness in a general setting, as

$$\begin{cases} Q(\theta)M\dfrac{d\mathbf{q}_N}{dt} + S\cdot\mathbf{F}_N - M\mathbf{S}(\theta)_N = F\hat{\mathbf{n}}\cdot[\mathbf{F}_N - \mathbf{F}^*], \\ \mathbf{q}_N(\mathbf{x},t=0,\theta) = \mathbf{f}(\mathbf{x},\theta), \end{cases} \tag{24}$$

where the initial conditions are given by the function $\mathbf{f} = \mathbf{f}(\mathbf{x},\theta)$ and the unknown vector $\mathbf{q}_N$ is given by (23). As a first step, we discretize (24) in the random space using a Galerkin approach. Multiplying (24) by a test function $\Psi_k(\theta)$, replacing $\mathbf{q}_N$ by its chaos expansion, and using the scalar product defined by (21), we obtain

$$\forall k \in [1,P] : \sum_{i=1}^{P} \langle Q\Psi_i,\Psi_k\rangle M\frac{d\mathbf{q}_N^i}{dt} + k!S\cdot\mathbf{F}_N^k - M\mathbf{S}_N^k = F\sum_{i=1}^{P}\hat{\mathbf{n}}\cdot[\mathbf{F}_N^i - \mathbf{F}^{i*}], \tag{25}$$

where we have used property (21). The detailed expression of the terms on the right-hand side is

$$\hat{\mathbf{n}} \cdot [\mathbf{F}_N^i - \mathbf{F}^{i*}] = \begin{pmatrix} \left\langle \overline{Z}^{-1}\Psi_i, \Psi_k \right\rangle \hat{\mathbf{n}} \times \hat{\mathbf{n}} \times [\mathbf{E}^i] - \left\langle Z^+\overline{Z}^{-1}\Psi_i, \Psi_k \right\rangle \hat{\mathbf{n}} \times [\mathbf{H}^i] \\ \left\langle \overline{Y}^{-1}\Psi_i, \Psi_k \right\rangle \hat{\mathbf{n}} \times \hat{\mathbf{n}} \times [\mathbf{H}^i] + \left\langle Y^+\overline{Y}^{-1}\Psi_i, \Psi_k \right\rangle \hat{\mathbf{n}} \times [\mathbf{E}^i] \end{pmatrix}. \tag{26}$$

Recall that $Z$ and $Y$ may depend on the material properties and, thus, may include uncertainty/randomness.

The initial conditions in (24) also need to be projected onto the chaos basis to give an initial condition for each mode of $\mathbf{q}_N^i$ in the chaos expansion, i.e.,

$$\forall i \in [1, P] \,:\, \mathbf{q}_N^i(\mathbf{x}, t=0) = \frac{1}{i!}\langle \mathbf{f}(\mathbf{x}, \theta), \Psi_i \rangle. \tag{27}$$

Once the vectors $\{\mathbf{q}_N^i\}_{1 \le i \le P}$ of the system (31) have been computed, we have available at every point in space an approximation to the probability density of the solution to the system.

Considering (31), we observe that we have managed to recast the general stochastic problem into a system of $P$ coupled deterministic problems which we can now discretize in space/time exactly as discussed in section 3—or in any other preferred way.

### 4.3 Stochastic collocation formulation

The idea of the stochastic collocation formulation is to replace the expression of the electric and magnetic fields (23) in the polynomial chaos expansion with a Lagrangian polynomial basis; i.e., we would have

$$\mathbf{q}(\mathbf{x}, t, \theta) = \sum_{i=1}^{P} \mathbf{q}^i(\mathbf{x}, t) L_i(\theta), \tag{28}$$

where $\{L_i(\theta)\}_{1 \le i \le P}$ forms a Lagrangian polynomial basis of degree $(P-1)$. In the deterministic community, (23) would be referred to as a modal expansion and (28) as a nodal expansion. Since $\theta$ in (28) is a Gaussian variable with zero mean and unit variance, it seems natural to use Gauss–Hermite collocation points as the basis for the Lagrange polynomials, as that also enables accurate evaluation of integrals.

The stochastic collocation method is essentially a deterministic or lattice Monte Carlo method with samples $\{\sqrt{2}\theta_j\}_{1 \le j \le P}$. The crucial difference is that a typical Monte Carlo simulation consisting of $P$ realizations will converge at the slow rate $1/\sqrt{P}$, whereas the convergence of the stochastic collocation method is much faster, as will be shown by numerical examples. A simple analogy is that the approximation of a smooth function, the PDF, is done most efficiently by representing it by smooth polynomials based on points well suited for interpolation. In a simple Monte Carlo approach, the interpolation points are random, leading to a poor convergence rate.

We presented the stochastic collocation method for a random space of size $d = 1$. The generalization to higher random spaces is straightforward, using tensor products of quadrature points. Note that for higher random spaces and for purposes of efficiency, it might be necessary to use sparse grid methods

### 4.4 Modelling of a random surface

We consider an object whose shape can vary in a random fashion. As an example, Figure 1 shows a disc which is modelled by $(n-1)$ line segments $[\mathbf{X}_i\mathbf{X}_{i+1}]_{1 \le i \le n-1}$ from a finite element mesh. Those

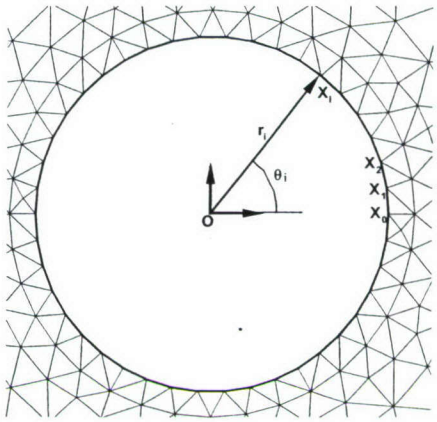


Figure 1: Points $X_i = (r_i \cos(\theta_i), r_i \sin(\theta_i))$ defining the boundary of an object.

line segments are defined by the points of polar coordinates $\mathbf{X}_i = (r_i \cos(\theta_i), r_i \sin(\theta_i))_{1 \leq i \leq n}$. We now assume that the point $\mathbf{X}_i$ can be moved randomly by a quantity $\delta\mathbf{X}_i = (\delta r_i \cos(\theta_i), \delta r_i \sin(\theta_i))_{1 \leq i \leq n}$ to take a new position $(\mathbf{X}_i + \delta\mathbf{X}_i) = ((r_i + \delta r_i)\cos(\theta_i), (r_i + \delta r_i)\sin(\theta_i))_{1 \leq i \leq n}$. We further assume that two points (say $\mathbf{X}_i$ and $\mathbf{X}_j$) with polar angles $\theta_i$ and $\theta_j$ close to each other should have a random height $\|\delta\mathbf{X}_i\|$ close to $\|\delta\mathbf{X}_j\|$. This is done by introducing the covariance matrix $\mathbf{K}$ such that:

$$K_{ij} = c^2 e^{-\frac{|\beta_i - \beta_j|}{b}}, \tag{29}$$

where

$$\beta_i = \begin{cases} \theta_i & if \quad \theta_i \in [0, \pi] \\ \pi - \theta_i & if \quad \theta_i \in ]0, 2\pi] \end{cases} \tag{30}$$

In the definition of $\beta_i$ we have to separate the cases $\theta_i \in [0, \pi]$ and $\theta_i \in ]0, 2\pi]$ to ensure that two points on the random surface, one with a polar angle close to 0 and the other one with a polar angle close to $2\pi$, be strongly correlated. In the relation (29), $b$ is a parameter which can control how correlated two points $\mathbf{X}_i$ and $\mathbf{X}_j$ can be and $c$ is another parameter which controls the roughness of the surface (the magnitude of $\|\delta\mathbf{X}_i\|$ for $i = 1, .., n$ is directly proportional to $c$). Furthermore, $c$ is the standard deviation of each component of $\delta\mathbf{r}$.

To generate a random surface, the problem can be formulated as follows: find a random vector $\delta\mathbf{r} = (\delta r_1, \delta r_2, ..., \delta r_n)^T$ with a given covariance matrix $\mathbf{K}$ that will generate the new random surface $(\mathbf{X}_i + \delta\mathbf{X}_i) = ((r_i + \delta r_i)\cos(\theta_i), (r_i + \delta r_i)\sin(\theta_i))_{1 \leq i \leq n}$. This procedure is illustrated in Figure 2, where a triangle $(A, \mathbf{X}_i, \mathbf{X}_{i+1})$ having one side $[\mathbf{X}_i\mathbf{X}_{i+1}]$ sitting on the boundary of the object is distorted into a new triangle $(A, \mathbf{X}_i + \delta\mathbf{X}_i, \mathbf{X}_{i+1} + \delta\mathbf{X}_{i+1})$ which side $[(\mathbf{X}_i + \delta\mathbf{X}_i)(\mathbf{X}_{i+1} + \delta\mathbf{X}_{i+1})]$ will compose the new shape of the object. From a practical point of view, this can be easily done by first generating a vector $\mathbf{G} = \sqrt{3}(\alpha_1, \alpha_2, ..., \alpha_n)^T$, where $\alpha_1, \alpha_2, ..., \alpha_n$ are random independent variables following (for example) a uniform law on the interval $[-1, 1]$. Since $\mathbf{K}$ is symmetric definite positive, it can be decomposed as $\mathbf{K} = \mathbf{PDP}^{-1}$, where $\mathbf{D}$ is a diagonal matrix with positive eigenvalues on its diagonal. Then, it can be shown that the vector $\delta\mathbf{r}$ given by $\delta\mathbf{r} = \mathbf{PD}^{1/2}\mathbf{G}$ will be a random vector

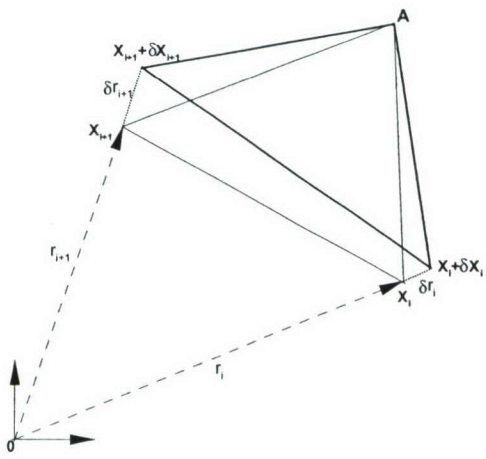


Figure 2: Illustration showing how the points on the boundary of an object are moved randomly.

with covariance matrix $\mathbf{K}$. In terms of implementation, one generates independents pseudo-random numbers $\alpha_1, \alpha_2, ..., \alpha_n$ with a uniform law on the interval $[-1, 1]$, then the vector $\delta\mathbf{r}$ is given by the matrix-vector product $\mathbf{PD}^{1/2}\mathbf{G}$ (the matrix $\mathbf{PD}^{1/2}$ can be pre-computed and stored once for all). The coordinates of the points of the new random surface will be $(\mathbf{X}_i + \delta\mathbf{X}_i)$ for $i = 1, ..., n$. The procedure described here for a disc can be easily adapted to objects with more general shapes, as will be shown in the numerical experiments section.

As an example, we have considered a somewhat simplified rocket in Figure 3. Figure 4 shows a zoom of its front part for the original (non-distorted) rocket and a typical sample mesh, when the procedure described above has been applied (here, we take $b = 5$ and $c^2 = 0.002$ in equation (29)). It should be noted that with this procedure, one just needs to generate a single mesh for the problem to be solved (the mesh of the object with its original shape, i.e. the mesh of Figure 3, for example). One needs to be careful that once the points defining the original object have been moved randomly, the triangles sitting on the object do not distort the mesh too much. This can be easily controlled by the parameter $c$ in equation (29) which is directly linked to the amplitude that $\delta r_i$ can take. The coordinates of the points which define the finite element mesh only occur in the matrices $\mathbf{M}$, $\mathbf{S}$, and $\mathbf{F}$ of equation (16) and those quantities are constant element by element. Since those matrices appear as multiplicative coefficients into Maxwell's equations we have transformed a problem with an object having a random shape (which usually requires the generation of a new mesh for each sample) into an equivalent stochastic problem having a fixed mesh but with random coefficients.

## 5 Computation of sensitivity of the RCS

The (2D) RCS under the scattering angle $\phi$, is a function of the following integral along $dC$ :

$$\begin{aligned} F(\phi) &= \frac{1}{2}e^{j\frac{\pi}{4}} \oint_{dC} \left[ \left( n_y \widetilde{H}_x - n_x \widetilde{H}_y \right) + \right. \\ &\quad \left. \left( n_x \cos\phi + n_y \sin\phi \right) \widetilde{E}_z \right] \\ &\quad e^{j2\pi f(x\cos\phi + y\sin\phi)} dl \end{aligned} \tag{31}$$

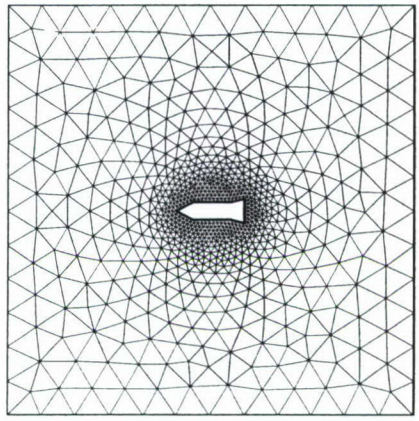

Figure 3: Original mesh for the rocket problem.

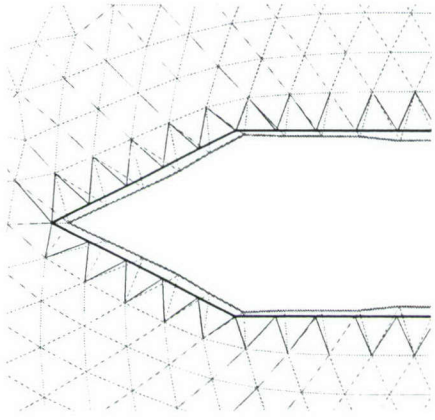

Figure 4: One sample of a mesh for the rocket with a random shape together with its original shape.

and normalized as

$$RCS(\phi) = 2\pi f \frac{|F(\phi)|^2}{|\mathbf{E}_0|^2},$$

where $\mathbf{E}_0$ is power of the incoming field. For the $2D$ calculations, a scaling equal to the wavelength $\lambda$ is applied to the RCS, i.e. the plots of the RCS on a $dB$ scale are simply

$$RCS_{dB}(\phi) = 10\log_{10}(RCS(\phi)/\lambda).$$

For the RCS for $3D$ scattering objects, a scaling equal to $\lambda^2$ is applied.

### 5.1 Using Monte-Carlo simulation

A Monte-Carlo simulation is therefore quite simple: one simply need to generate (say) $M$ random vectors $\{\delta\mathbf{r}_m\}_{1\leq m\leq M}$ as described above. Each set of random numbers will give a new random surface from which we can compute $M$ solutions of Maxwell's equations. Those $M$ solutions of Maxwell's equations, will give $M$ radar cross section $\{RCS_m\}_{1\leq m\leq M}$ from which we can compute averages as follows:

$$< RCS >= \frac{1}{M}\sum_{m=1}^{M} RCS_m. \tag{32}$$

And for the variance, we have

$$var(RCS) = \frac{1}{M}\sum_{m=1}^{M} (RCS_m)^2 - < RCS >^2 . \tag{33}$$

It should be noted that the advantage of the Monte-Carlo approach is its simplicity (it only requires repetitive runs of an existing deterministic solver), but it is hard to get accurate solutions due to its slow rate of convergence $O(M^{-1/2})$. In the next subsection, we will introduce a stochastic collocation method which has the simplicity of the Monte-Carlo approach but with better rates of convergence.

### 5.2 Computation of sensitivity of RCS using stochastic collocation

About fifty years ago, Stroud constructed a set of cubature points to compute integrals of the form

$$I[f] = \int_{[-1,1]^n} f(\mathbf{x})d\mathbf{x}. \tag{34}$$

This set of cubature points based on $(n+1)$ points is exact for polynomials of degree two, and the approximation is written as

$$I[f] \simeq \sum_{i=1}^{n+1} \omega_i f(\mathbf{x}_i), \tag{35}$$

where the $(n+1)$ cubature points $\mathbf{x}_i = (x_i^1, x_i^2, ..., x_i^n)$ are given by

$$\begin{aligned} x_i^{2r-1} &= \sqrt{\frac{2}{3}}\cos\left(\frac{2r(i-1)\pi}{n+1}\right), \\ x_i^{2r} &= \sqrt{\frac{2}{3}}\sin\left(\frac{2r(i-1)\pi}{n+1}\right), \end{aligned} \tag{36}$$

for $r = 1, ..., [n/2]$, and if $n$ is odd, $x_i^n = (-1)^{(i-1)}/\sqrt{3}$. The weights in (35) are all equal to $2^n/(n+1)$. Similarly, we have the Stroud-3 method based on $2n$ points which is exact for polynomials of degree three :

$$I[f] \simeq \sum_{i=1}^{2n} \omega_i f(\mathbf{x}_i), \tag{37}$$

where the $2n$ cubature points $\mathbf{x}_i = (x_i^1, x_i^2, ..., x_i^n)$ are now defined by

$$\begin{aligned} x_i^{2r-1} &= \sqrt{\frac{2}{3}} \cos\left(\frac{(2r-1)i\pi}{n}\right), \\ x_i^{2r} &= \sqrt{\frac{2}{3}} \sin\left(\frac{(2r-1)i\pi}{n}\right), \end{aligned} \tag{38}$$

for $r = 1, ..., [n/2]$ and if $n$ is odd, similarly we have, $x_i^n = (-1)^i/\sqrt{3}$. The weights in (37) are all equal to $2^n/2n$. It can be shown that Stroud-2 and Stroud-3 methods employ the minimal number of points for their corresponding integration accuracy. Since Stroud-2 and Stroud-3 methods appeared, many other cubature formulae have been established to compute various high-dimensional integrals. In the 70's, Stroud published a book containing most cubature formulae known at that time. This extensive work was then continued by Cools in a series of two papers. The idea of the stochastic collocation method is based on polynomial interpolations in the multi-dimensional random space. We assume that Lagrange polynomials based on Stroud's cubature points exist, and we express the RCS using the Lagrange interpolation polynomials, which gives (for Stroud-2 cubature points)

$$RCS(\mathbf{x}) = \sum_{i=1}^{n+1} RCS_i L_i(\mathbf{x}), \tag{39}$$

where $\{L_i\}_{1 \le i \le n+1}$ are $(n+1)$-variate Lagrange polynomials based on points $\{\mathbf{x}_i\}_{1 \le i \le n+1}$ of the cubature formula (35). We note that by construction of Lagrange polynomials, we have $L_i(\mathbf{x}_j) = \delta_{ij}$ and therefore $RCS_i = RCS(\mathbf{x}_i)$. The radar cross sections $RCS(\mathbf{x}_i)$ can be easily computed as follows:

- for each cubature point $\mathbf{x}_i$ generate a new surface with $\delta\mathbf{r}_i = \mathbf{P}\mathbf{D}^{1/2}\mathbf{G}_i$ and $\mathbf{G}_i = \sqrt{3}\mathbf{x}_i$ $(i = 1, ..., n+1)$
- compute the corresponding solution of Maxwell's equations
- compute the corresponding radar cross section $RCS(\mathbf{x}_i)$

The expression of the RCS is now available under the form (39) and we will show that statistical quantities, e.g. mean and variance, can easily be computed. By taking the average of equation (39) and evaluating the multi-dimensional integral with Stroud-2 cubature formula (35), we get

$$\begin{aligned} < RCS(\mathbf{x}) > &= \frac{1}{2^n} \sum_{i=1}^{n+1} RCS_i \int_{[-1,1]^n} L_i(\mathbf{x}) d\mathbf{x} \\ &= \frac{1}{2^n} \sum_{i=1}^{n+1} RCS_i \sum_{j=1}^{n+1} \omega_j L_i(\mathbf{x}_j) \end{aligned}$$

$$= \frac{1}{2^n}\sum_{i=1}^{n+1} RCS_i \sum_{j=1}^{n+1} \omega_j \delta_{ij}$$
$$= \frac{1}{2^n}\sum_{i=1}^{n+1} \omega_i RCS_i$$

Similarly, for the variance, we have

$$var(RCS(\mathbf{x})) = \frac{1}{2^n}\sum_{i=1}^{n+1} \omega_i {RCS_i}^2 - < RCS(\mathbf{x}) >^2 . \tag{40}$$

The same procedure can be used with Stroud-3 cubature, and in that case, $2n$ realizations of the RCS corresponding to the $2n$ cubature points of equation (37) will have to be computed. When the random space is one-dimensional this procedure can also be repeated for the Legendre-Gauss-Lobatto quadrature.

Alternatively, we could have used orthogonal polynomials to express the RCS, i.e. equation (39) would have to be replaced by

$$RCS(\mathbf{x}) = \sum_{i=1}^{n+1} RCS_i \Phi_i(\mathbf{x}), \tag{41}$$

where $\Phi_i(\mathbf{x})$ are orthogonal polynomial on $[-1,1]^n$. The expression (41) is usually referred as "polynomial chaos expansion" and was used in a number of mechanical problems. The problem of this approach lies in the difficulty to compute in an efficient way the coefficients $RCS_i$.

### 5.3 Reduced random space

For the stochastic collocation method, we have seen that there is a close relation between the size of the random space $n$ and the number of calls to the deterministic Maxwell solver (i.e. we need $(n+1)$ calls for Stroud-2 and $2n$ calls for Stroud-3). A way of reducing the CPU cost of the method would be to reduce the size of the random space $n$. This is possible, up to a certain extent, depending on the covariance matrix $\mathbf{K}$ defined by equation (29). Let us consider the two extreme cases:

First, we assume that $b \to 0$ and $c = 1$ in equation (29); in this case, $\mathbf{K} = \mathbf{I}$ is the identity matrix and $\mathbf{P} = \mathbf{D} = \mathbf{I}$. In other words we will need $n$ independent and identically distributed random variables to describe the process since all points of the object are uncorrelated.

Now we assume that $b \to \infty$ and $c = 1$ in equation (29); in this case, all variables are fully correlated. We have $K_{ij} = P_{ij} = 1$ for $i, j = 1, ..., n$; $D_{11} = 1$ and $D_{ii} = 0$ for $i = 2, ..., n$. Thus, all $n$ points of the sample $\delta\mathbf{r} = (\delta r_1, \delta r_2, ..., \delta r_n)^T = \mathbf{P}\mathbf{D}^{1/2}\mathbf{G}$ are moved with the same amplitude, i.e. $\delta r_1 = \delta r_2 = ... = \delta r_n$. This means that $n = 1$ would suffice to describe the problem. In practice, we are between those two extreme cases and the size of the random space can be given by the number of significant eigenvalues of $\mathbf{D}$ denoted by $m$ (with $m \leq n$). Then, the modified algorithm proceeds as follows:

- Compute the $n$ eigenvalues $\{\lambda_i\}_{1 \leq i \leq n}$ of the matrix $\mathbf{K}$ and select the $m$ most significant ones satisfying $\left|\frac{\lambda_i}{\lambda_{\max}}\right| \geq TOL$, where $TOL$ is some small number. The integer $m$ will be the size of the random space needed to move the points of the objects randomly.

- We denote by $\widetilde{\mathbf{P}}$ and $\widetilde{\mathbf{D}}$ the matrices of size $n \times m$ constructed from the restriction of the matrices $\mathbf{P}$ and $\mathbf{D}$ where we have only kept the most significant eigenvalues and their associated eigenvectors.
- Since the dimension of the random space is reduced to $m \leq n$, the collocation points $\mathbf{x}$ are $m$-dimensional vectors based on quadrature points for the computation of $m$-dimensional integrals. For Stroud-2, we have $(m+1)$ points and for Stroud-3, it is $2m$.
- The vector $\delta\mathbf{r}$ used to move the mesh is now given by $\delta\mathbf{r} = (\delta r_1, \delta r_2, ..., \delta r_n)^T = \widetilde{\mathbf{P}}\widetilde{\mathbf{D}}^{1/2}\mathbf{G}$, where $\mathbf{G} = \sqrt{3}\mathbf{x}$.

# 6 A few examples

We now consider a square of width $0.8\lambda$ whose mesh consists of 840 elements. Again, $\lambda$ is the wavelength of the incident plane wave. The dimension of the full random space is 44, which means that the square is formed by 44 points of the finite element mesh. The parameters $b$ and $c^2$ in equation (29) are taken equal to 5 and 0.001, respectively. This choice of $c$ corresponds to the radial randomness having a standard deviation of about $0.032\lambda$. By choosing $b = 5$, the covariance matrix $\mathbf{K}$ defined by (29) is more diagonal dominant than it was in the previous example, and the number of most significant eigenvalues is reduced to $m = 16$. Due to the geometrical singularities in the corners of the square, this is a much harder problem to solve than the cylinder problem. This is illustrated on Figure 5 and 6, where we show the mean and the variance of the RCS for the Stroud-2, the Stroud-3 and the Monte-Carlo methods using 250 samples. We can see on Figure 5 that the mean converges to the same values for the three methods. However, for the variance, the Stroud-3 and the Monte-Carlo methods give similar results but the Stroud-2 method gives results which have not converged, especially in the sidebands. This is because Stroud-2 can only integrate exactly multi-variate polynomials of degree two at most, and the exact solution of this example cannot be accurately represented by such polynomials. On the other hand, Stroud-3 which can integrate exactly multi-variate polynomials of degree three at most does a better job. In order to emphasize the cost saving of Stroud-3 method over Monte-Carlo method, we have represented the variance of the RCS for Stroud-3, Monte-Carlo with 32 samples (which has the same CPU-cost as the Stroud-3 method) and Monte-Carlo with 250 samples in Figure 7. We see that as we increase the number of samples, the Monte-Carlo solution converges slowly to the Stroud-3 solution. Figure 8 shows the average of the RCS and the possible variations around its average value obtained with Stroud-3 cubature. We can see that like for the cylinder problem, the uncertainty in shape affects the RCS mostly in the sidebands.

## 6.1 General shape

As a last shape, we consider the (simple) rocket shown in Figure 3 which is $\lambda$ long and the body is $0.25\lambda$ wide. The mesh consists of 1465 elements and the dimension of the full random space is 45 (i.e. the rocket is formed by 45 points of the finite element mesh). As for the square problem, the parameters $b$ and $c^2$ in equation (29) are taken equal to 5 and 0.001, respectively and the size of the random space can be reduced to $m = 14$. This choice of $c$ corresponds to the radial randomness having a standard deviation of about $0.032\lambda$. Similarly to the square problem, good convergence of the average RCS is obtained both for Stroud-2, Stroud-3 and Monte-Carlo simulations. However for the variance of the RCS, only Stroud-3 and Monte-Carlo with enough samples (i.e. more than 250) give good results. Figure 9 shows the average of the RCS and the possible variations around

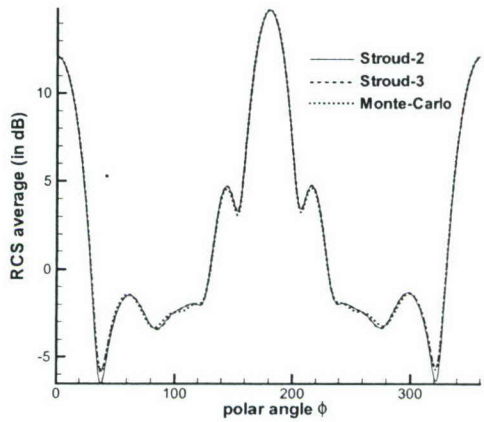


Figure 5: Comparison of the average of the RCS for the square problem for Stroud-2, Stroud-3 and Monte-Carlo methods.

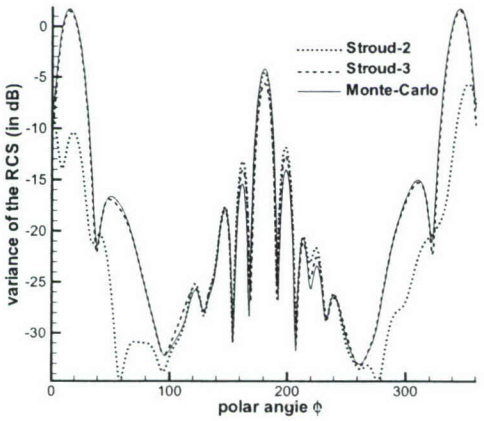


Figure 6: Comparison of the variance of the RCS for the square problem using Stroud-2, Stroud-3 and Monte-Carlo methods.

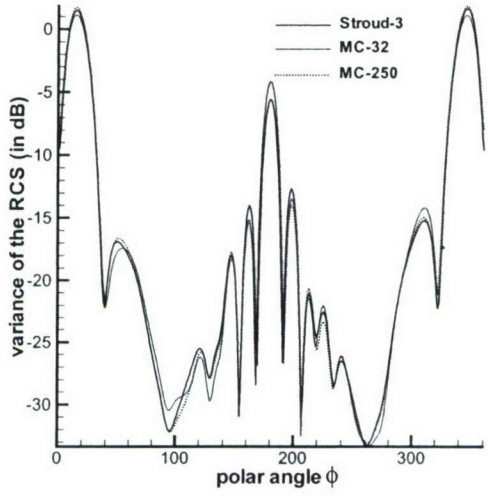


Figure 7: Comparison of the variance of the RCS for the square problem using Stroud-3 method and Monte-Carlo method with 32 and 250 samples.

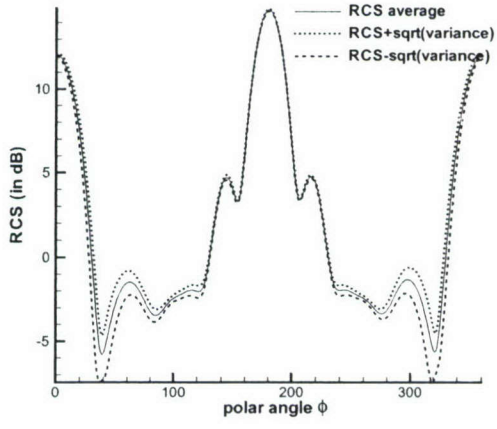


Figure 8: RCS for the square problem. Results are shown with the mean RCS as well as $\pm$ one standard deviation.

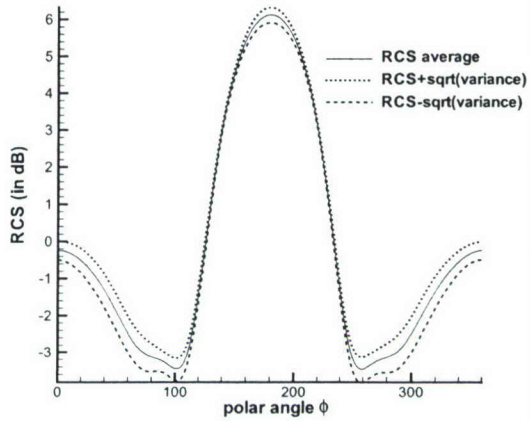


Figure 9: RCS for the rocket problem. Results are shown with the mean RCS as well as $\pm$ one standard deviation.

its average value obtained with Stroud-3 cubature. For this case, the uncertainty in shape affects the RCS both in the middle part and in the sidebands.

### 6.2 Higher frequency cases

As a last numerical experiment in two spatial dimensions, we increase the frequency $f$ of the source term (??) up to $f = 3$. This causes the radius of the cylinder to increase to $3\lambda$ and the size of the rocket to increase to $3\lambda$ long and $0.75\lambda$ wide in the body. For these cases the radial randomness has a standard deviation of about $0.095\lambda$. For all the previous numerical experiments, we have used 4th order elements in each triangle of the finite element grid. Due to the higher frequency, all the results shown in this section are obtained with 6th order elements to get converged results in the physical space (i.e. the value of $p$ defined below equation (11) is increased to $p = 6$). Figures 10 and 11 show the average of the RCS and the possible variations around its average value obtained with Stroud-3 cubature for the cylinder and the rocket problem, respectively. The form of the uncertainty remains the same as in the previous numerical examples, the only difference being the frequency of the source term. By comparing Figure ?? with Figure 10 and Figure 9 with Figure 11, we see that as we increase the frequency, the regions where the RCS has the greatest variance remains more or less the same. In this numerical experiment, convergence of the average of the RCS and the variance of the RCS is good for the cylinder problem, for both Stroud and Monte-Carlo methods. However, for the rocket problem only Stroud-3 and Monte-Carlo with enough samples give converged results for the variance.

### 6.3 Sphere

For a first example with three spatial dimensions we consider the scattering of a transverse magnetic plane wave from a PEC sphere. We assume the sphere has a uniform random radius in the interval $[0.9\lambda, 1.1\lambda]$, where $\lambda$ is the wavelength of the incident field. The use of one random variable is not a limitation of the method but is done for logistical reasons to have reasonable computation times. Since this experiment has only one random dimension, a sixth order Legendre-Gauss-Lobatto

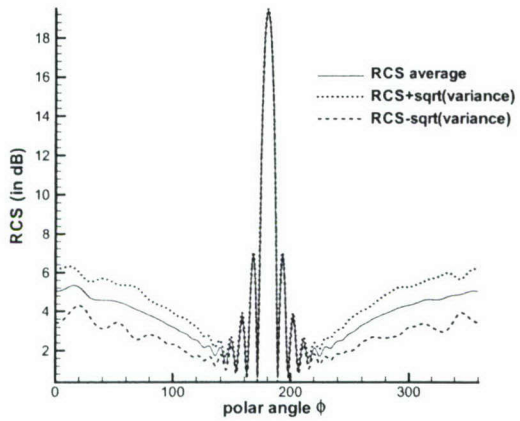


Figure 10: RCS for the cylinder problem at higher frequency. Results are shown with the mean RCS as well as $\pm$ one standard deviation.

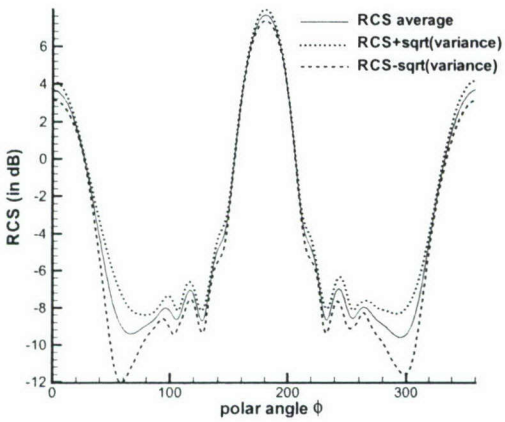


Figure 11: RCS for the rocket problem at higher frequency. Results are shown with the mean RCS as well as $\pm$ one standard deviation.

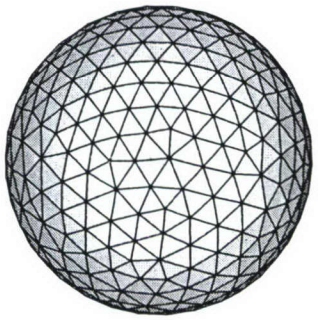

Figure 12: One sample of a surface mesh for the sphere with a random radius.

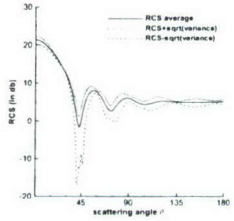


Figure 13: RCS for the sphere problem. Results are shown with the mean RCS as well as $\pm$ one standard deviation.

quadrature is used for collocation in the random space. For the spatial discretization we use fourth order elements and a sample mesh is presented in Figure 12 which is restricted to the surface of the sphere. Figure 13 shows the average of the RCS and the possible variations around its average value. The uncertainty in the radius of the sphere affects the RCS mainly in the sideband.

### 6.4 Three-dimensional rocket

For the second experiment with three spatial dimensions we consider the scattering of a transverse magnetic plane wave from a PEC rocket. The orientation of the scattering plane and the scattering angle $\theta$ is is given in Figure 14 along with a geometric description of the rocket. The scattering angle of the incident field is assumed to be random with uniform distribution in the interval $[10°, 20°]$. As in the case for the sphere, the use of one random variable is not a limitation of the method but is done for logistical reasons to have reasonable computation times. A fourth Legendre-Gauss-Lobatto is used for collocation in the one-dimensional random space. For this calculation the physical space is discretized with degree five polynomials in each element. Figure 15 shows the mesh used restricted

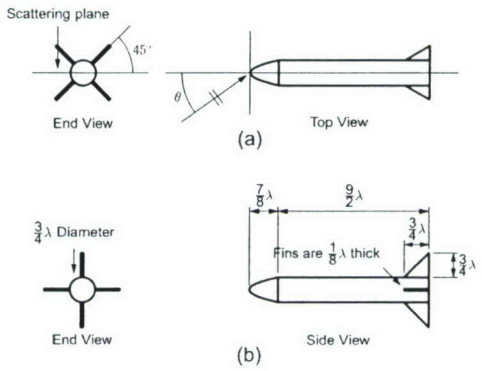


Figure 14: The orientation of the rocket with respect to the scattering plane is given in (a). Here $\theta$ is the scattering angle. The top view presents a projection of the rocket onto the scattering plane. The geometric description of the three-dimensional rocket is given in (b). Here $\lambda$ is the wavelength of the incident field.

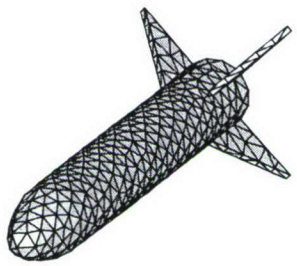

Figure 15: The surface mesh for the three-dimensional rocket.

to the surface of the rocket and Figure 16 shows the average of the RCS and the possible variations around its average value. The uncertainty in the direction of the incident field affects the RCS mainly near the local maxima and minima points of the RCS.

# 7 People involved in project

- PI: Jan S Hesthaven, Brown University
- Student: Dr Lucas Wilcox (PhD'06, US citizen). Currently postdoc at ICES, UT Austin
- Student: Dr Laura Lurati (PhD'06, US citizen). Current postdoc at Boeing Phantom Works and the Institute of Mathematics and it Applications (IMA).
- Student: Mr Akil Narayan (PhD expected 2009, US citizen)
- Consultant: Professor Tim Warburton, Rice University

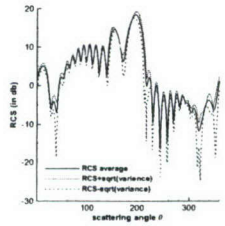


Figure 16: RCS for the three-dimension rocket problem. Results are shown with the mean RCS as well as $\pm$ one standard deviation.

- Collaborator: Professor Cedric Chauviere, University Blaire Pascal, France
- Collaborator: Professor Dongbin Xiu, Purdue University

# 8 Publications


- J. S. Hesthaven and T. Warburton, 2004, *High-Order Accurate Methods for Time-domain Electromagnetics*, Comp. Mod. Engin. Sci. **5**(5), 395–408.
- Q. Y. Chen, D. Gottlieb, and J. S. Hesthaven, 2005, *Uncertainty Analysis for Steady-State Inviscid Burgers Equation.* J. Comput. Phys. **204**, pp. 378-398.
- D. Xiu and J.S. Hesthaven, 2005, *High-Order Collocation Methods for Differential Equations with Random Inputs*, SIAM J. Sci. Comput. **27**, pp. 1118-1139.
- C. Chauviere, J.S. Hesthaven, and L. Lurati, 2006, *Computational Modeling of Uncertainty in Time-Domain Electromagnetics*, SIAM J. Sci. Comp. **28**(2), pp. 751-775.
- S. Abarbanel, D. Gottlieb, and J. S. Hesthaven, 2006, *Nonlinear PML for Electromagnetics*, J. Sci. Comput **28**(2-3),pp. 125-137.
- T. Warburton, *An Explicit Construction for Interpolation Nodes on the Simplex*,Journal of Engineering Mathematics **56**(2006), pp. 247-262.
- T. Warburton and M. Embree, *On the Role of the Penalty in the Local Discontinuous Galerkin Method for Maxwell's Eigenvalue Problem*, Computer Methods Applied Mechanical Engineering, Vol **195**(2006), pp. 3205-3223.
- C. Chauviere, J.S. Hesthaven, and L. Wilcox, 2007, *Efficient Computation of RCS from Scatters of Uncertain Shapes*, IEEE Trans. Antennas Propagat. **55**(5), pp. 1437-1448.

## 9 Presentations

**Conference talks** PIERS Meeting, Pisa, Italy (04/04); CRM Scientific Computing Days, Montreal (02/05); Frontiers in Applied and Computational Mathematics, NJIT, NJ (05/05); Computational Electromagnetics in the Time-Domain, 2005. CEM-TD 2005, Georgia Tech (09/05); Norwegian Research Foundation Fall Meeting in Computational Mathematics (BeMATA), Oslo, Norway (10/05); ACES Conference on CEM, Verona, Italy (03/07); ICOSAHOM 2007, Beijing, China (06/07);

**University seminars** Sandia National Laboratory (05/2004); Kirtland AFB (05/2004). INRIA-Rocquencourt; France (07/2004); INRIA-Sophia-Antipolis, Nice, France (07/2004);University of Texas, El Paso (11/2004); Uppsala University, Sweden (2/2005); Ohio State University, Columbus (3/2005); Technical University of Denmark, Department of Mechanical Engineering (04/06); ONERA, Paris, France (04/06); Xi'an Jian Tong University, Department of Mathematics, Xi'an, China (6/07)

## 10 Transition

As outlined in the original proposal, it was planned that some of the techniques being developed in this effort be implemented into the TEMPUS CEM code, developed and maintained by HyperComp, Inc and used extensively for RCS prediction and modeling by DoD contractors and laboratories.

This has been accomplised and we stay in continued close contact, The PI has visited HyperComp several times during the period to report on progress and discuss ways of implementing the developed techniques into TEMPUS which now has elementary support for uncertainty quantification During the effort, we have also stayed in close contact with WPWFB (Dr Camberos) to update him on status and enable a possible future transition of the technology to their internal simulation framework.